

High-Density Ceramics of $Al_{2-x}Me_x(WO_4)_3$, (Me = Sc or In) Solid Solutions

Iovka Koseva*, Aneliya Yordanova, Velin Nikolov

Institute of General and Inorganic Chemistry, Bulgarian Academy of Sciences, Sofia, Bulgaria.
Email: *ikosseva@svr.igic.bas.bg, a.yordanova@svr.igic.bas.bg, vnikolov@svr.igic.bas.bg

Received August 26th, 2013; revised September 26th, 2013; accepted October 3rd, 2013

Copyright © 2013 Iovka Koseva *et al.* This is an open access article distributed under the Creative Commons Attribution License, which permits unrestricted use, distribution, and reproduction in any medium, provided the original work is properly cited.

ABSTRACT

$Al_{2-x}Me_x(WO_4)_3$, (Me is Sc or In; x varies from 0 to 2) ceramics are sintered by two methods: 1) cold pressing with subsequent sintering at different temperatures and durations and 2) hot pressure sintering. The raw materials are nanoparticles with average particle size of 20, 90 and 200 nm obtained by co-precipitation method. Density, particle size and anisotropy of the obtained ceramics are tested. The results show that optimal initial nanosized dimensions and optimal pressing conditions are needed to obtain compact ceramics. The hot pressure method provides possibilities for obtaining ceramics with a density of about 99.8%. These ceramics possess some level of transparency.

Keywords: Ceramics; Sintering; Compaction; Electron Microscopy (SEM)

1. Introduction

Aluminium tungstate $Al_2(WO_4)_3$, indium tungstate $In_2(WO_4)_3$ and scandium tungstate $Sc_2(WO_4)_3$ belong to the class of compounds of the general formula $Me_2(WO_4)_3$, (Me = Y, Sc, In, Al or lanthanoids with small ionic radii—Ho, Er, Tm, Yb, and Lu) with orthorhombic structure, space group $Pnca$ [1]. This class of compounds possesses Al^{3+} ion conductivity which affords their use as solid electrolytes, sensors, etc. [2-4]. Some of the $Me_2(WO_4)_3$ compounds possess unusually low thermal expansion coefficients (including zero and even negative values) within a broad temperature range [5-7]. A further potential application of these tungstates is their use as active media for lasers. $Me_2(WO_4)_3$ compounds doped by Cr^{3+} are very prospective laser media for tunable lasers. The active Cr^{3+} ion possesses both broad absorption cross-section and broad emission cross-section when incorporated in a structure with weak or medium strong crystal field, as that displayed by $Me_2(WO_4)_3$ tungstates.

Being isostructural, these tungstates can form solid solutions. This is a very important advantage because it enables varying the coefficient of expansion, the ionic conductivity and the laser properties in a wide range by varying the chemical composition of the solid solution [8-10].

The elaboration of ionic conductors and materials with tailored expansion coefficients requires high-density ceramics.

The production of single crystals for laser active media from these tungstates is related to a number of problems mainly due to the significant evaporation of WO_3 in the case of Czochralski growth. When the crystals are grown by a flux method, the process is characterized by low growth velocity and high anisotropy of the crystals [11-17].

An effective approach to avoid those problems is to produce high-density ceramics instead of single crystals. If the density of the ceramics is close to the crystallographic one, transparent ceramics could be obtained. Moreover, transparent ceramics are low-cost products which possess high chemical homogeneity and isotropy [18].

The focus of our research in recent years was the preparation of high-density (transparent) ceramics of tungstates with the general formula $Al_{2-x}Me_x(WO_4)_3$, where Me is Sc or In, and x varies from 0 to 2. To our knowledge, preparation of high-density transparent tungstate ceramics has not been published yet.

The technology of optical ceramics production includes three main stages: 1) fabrication of nanopowders; 2) preparation of high-density compacts and 3) sintering the compacts in order to obtain non-porous ceramics [19]. Many investigations show that the fabrication of trans-

*Corresponding author.

parent ceramics needs ultrafine, monosized low-agglomerated nanopowders with high sintering activity [20-24].

The preparation of aluminium tungstate $\text{Al}_2(\text{WO}_4)_3$, indium tungstate $\text{In}_2(\text{WO}_4)_3$, scandium tungstate $\text{Sc}_2(\text{WO}_4)_3$ and solid solutions in the systems of $\text{Al}_2(\text{WO}_4)_3$ - $\text{In}_2(\text{WO}_4)_3$ and $\text{Al}_2(\text{WO}_4)_3$ - $\text{Sc}_2(\text{WO}_4)_3$ nanopowders was previously investigated. Pure phase nanopowders with mean particle size in the range of 10 - 200 nm were obtained and thoroughly characterized by X-ray, TEM, SEM, NMR, IR and Raman analysis [25-27].

In this article, we present the next step of the procedure cold pressing with additional sintering of the high-density compacts or hot pressure sintering.

2. Experimental

Nanosized powders of $\text{Al}_2(\text{WO}_4)_3$, $\text{Sc}_2(\text{WO}_4)_3$, $\text{In}_2(\text{WO}_4)_3$ and solid solutions of $\text{AlSc}(\text{WO}_4)_3$, $\text{AlIn}(\text{WO}_4)_3$ were obtained using the co-precipitation method. The amorphous precipitates of the samples were thermally treated at different temperatures and durations with a view to obtaining nanosized particles with average particle size of 20, 90 and 200 nm. Tungstates obtained by classical solid state synthesis, with an average particle size of 2 μm , were used as a reference.

To obtain high-density ceramics from these tungstates two methods were used:

-cold pressing followed by thermal sintering;

-hot pressure sintering followed by vacuum treatment.

For the cold pressing process a laboratory press with pressure of 600 MPa was used. Pellets with a diameter of 10 mm and thickness of 1.5 - 2 mm were prepared. The preliminary tests showed that the temperature, at which initial shrinkage begins, mainly depends on tungstate composition. For $\text{Al}_2(\text{WO}_4)_3$, $\text{Sc}_2(\text{WO}_4)_3$, $\text{In}_2(\text{WO}_4)_3$, $\text{AlSc}(\text{WO}_4)_3$ and $\text{AlIn}(\text{WO}_4)_3$, the initial shrinking temperature was 780°C, 680°C, 660°C, 760°C and 770°C, respectively. Therefore, the density of the pellets and the particle size was measured after thermal treatment for 1, 5 and 10 hours at 800°C, 900°C and 1000°C for $\text{Al}_2(\text{WO}_4)_3$, $\text{AlSc}(\text{WO}_4)_3$ and $\text{AlIn}(\text{WO}_4)_3$, and at 700°C and 800°C for $\text{Sc}_2(\text{WO}_4)_3$ and $\text{In}_2(\text{WO}_4)_3$.

Density measurements were carried out using Archimedes' principle. The liquid used was distilled water at 20°C, (density 0.99823 g/cm³). The density of the objects was calculated using the following formula:

$$A\rho(p) = \frac{M(p \cdot a)}{M(p \cdot a) - M(p \cdot w)} \cdot \rho(w),$$

where

$\rho(p)$: pellet density (g/cm³)

$M(p \cdot a)$: pellet weight measured in air (g)

$M(p \cdot w)$: pellet weight measured after being dipped in water (g)

$\rho(w)$: water density (g/cm³)

The accuracy of the pellets mass measurement was ± 0.001 g. Hence, the accuracy of the density calculation was ± 0.02 g/cm³.

The densities of the non-deformed pellets were calculated by dividing the measured mass by pellets volume. The diameter and the thickness of the samples were measured by a micrometer screw gauge (2 μm accuracy). The accuracy of the measurement in this case was ± 0.015 g/cm³. The samples obtained after sintering without any additional treatment of the surface were subjected to SEM analysis. The SEM micrographs with magnification of 200 - 5000 were obtained on a Philips SEM 515 device at an accelerating voltage of 20 kV. The powders were covered with a gold layer of 10 - 15 nm thickness.

The average particle size and the anisometricity were determined using Lince v2.4—Linear Intercept Program.

For hot pressure sintering a laboratory press applying simultaneous or separate pressure up to 100 MPa at temperatures up to 800°C was used. The pressure was applied in step mode (25, 50 or 100 MPa); the temperature was programmed with a speed from 20°C to 500°C per hour. Ceramic matrix with diameter of 10 mm was used. The nanosized powders of $\text{Al}_2(\text{WO}_4)_3$, $\text{Sc}_2(\text{WO}_4)_3$, $\text{In}_2(\text{WO}_4)_3$ and the solid solutions $\text{AlSc}(\text{WO}_4)_3$, $\text{AlIn}(\text{WO}_4)_3$ were subjected to hot pressure sintering. Samples with different composition and different particle size were hot pressed at different pressures (50 - 100 MPa) and different temperatures (400°C, 600°C and 800°C) for different pressing times (30 min, 1 h and 2 h). Some of the obtained nanosized powders were subjected to step-wise applying of pressure and temperature –25 MPa and 400°C for 15 min, followed by 50 MPa and 600°C for 15 min and 100 MPa and 800°C for 30 min. Density measurements were carried out by the methods already described. Samples with densities exceeding 98% of the crystallographic one were subjected to additional vacuum sintering at 1000°C for 2 h at a constant vacuum of 1 mm Hg.

3. Results and Discussion

3.1. Cold Pressing

Figure 1 presents the pellets compaction, the particle size and the level of anisometricity of $\text{Al}_2(\text{WO}_4)_3$, depending on sintering temperature (800°C, 900°C, 1000°C) for pellets with initial particle size of 20, 90, 200 nm (prepared by co-precipitation) and over 1 μm (prepared by classical solid state synthesis). Pellets density was presented as a relative value to the crystallographic one (5.079 for $\text{Al}_2(\text{WO}_4)_3$).

It can be seen that $\text{Al}_2(\text{WO}_4)_3$ obtained by the co-precipitation method with initial particle size of 20 nm, (Al20) and 90 nm (Al90), subjected to sintering at 800°C,

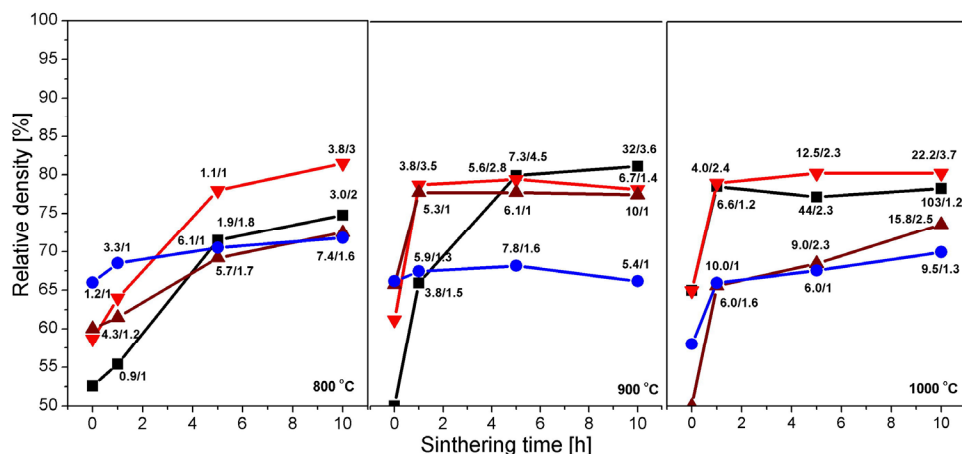


Figure 1. Variation of the relative density of $\text{Al}_2(\text{WO}_4)_3$ pellets, depending on sintering temperature (800°C, 900°C and 1000°C), sintering time (0, 1, 5 and 10 h) and average particle size in the raw pellets (—■— 20 nm, —▼— 90 nm, —▲— 200 nm and —●— >1 μm). 3.8/3 - 3.8 is the average particle size after appropriate sintering [μm]; 3 is the average ratio between the largest and the smallest particle size.

were compacted progressively with time, achieving 74%, respectively 81% of the crystallographic density. The compaction level is significantly lower for $\text{Al}_2(\text{WO}_4)_3$ with particle size of 200 nm (Al200) and for the sample obtained by classic solid state synthesis, with particles size of over 1 μm (Al1000). The latter one has only 68% of the crystallographic density. The time required for maximum compaction at 900°C for all samples was 1 h, except for Al20. Al20 and Al90 achieved the highest density 79% - 81% of the crystallographic one. After thermal treatment at 1000°C the highest density was achieved for Al20 and Al90 after 1 h of treatment—75% - 80%.

SEM micrographs of some samples are shown in **Figures 2-4**. These figures show that samples Al20 (**Figure 2**) and Al90 (**Figure 3**) have a very high sintering ability, compared to Al1000 (**Figure 4**). This ability is demonstrated by the very high speed of particle size growth during the thermal treatment. For example, the particle size of samples with initial average size of 20 nm (Al20) grows to 3.0, 32 and 103 μm upon treatment for 10 h at 800°C, 900°C and 1000°C, respectively. The particles in the pellets with initial size of 90 nm grow to 3.8, 6.7 and 22.2 μm at 800°C, 900°C and 1000°C, respectively.

In other words, the dimensions of the particles increase by a factor of 5000 for Al20 and 250 for Al90. Samples obtained by solid state synthesis (Al1000) possess significantly lower sintering ability. **Figure 4** illustrates the particles growth of Al1000. They grow from 2 μm to 5 - 10 μm .

The main reason for the relatively high compaction level of Al20 and Al90 seems to be just this sintering ability, which is expressed by a high growth speed of the particles.

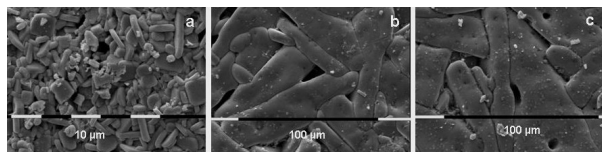


Figure 2. SEM photographs of the surfaces of the $\text{Al}_2(\text{WO}_4)_3$ pellets with initial average particle size of 20 nm after cold pressing and thermal treatment during 10 h at 800°C (a); 900°C (b) and 1000°C (c).

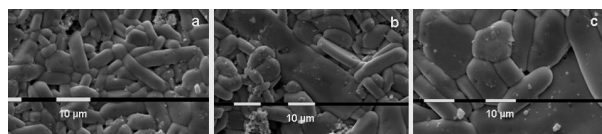


Figure 3. SEM photographs of the surfaces of the $\text{Al}_2(\text{WO}_4)_3$ pellets with initial average particle size of 90 nm after cold pressing and thermal treatment during 10 h at 800°C (a); 900°C (b) and 1000°C (c).

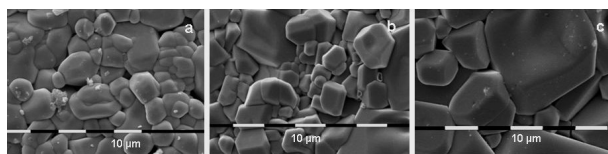


Figure 4. SEM photographs of the surfaces of the $\text{Al}_2(\text{WO}_4)_3$ pellets with initial average particle size of 2 μm after cold pressing and thermal treatment during 10 h at 800°C (a); 900°C (b) and 1000°C (c).

The SEM micrographs show another feature of the Al20 and Al90 samples. There is a clear tendency for growing of the grain in the preferable crystallographic direction (anisometricity). This tendency is more obvious for Al20, than for Al90 (**Figures 2** and **3**). Another feature is the tendency of habit growth for Al1000 (**Figure 4**). These features could explain the results on pellets

compaction. Al20 and Al90 display high sintering ability which leads to rapid particle growth and compaction. The higher tendency of anisometric growth of Al20 compared with Al90 could explain the higher compaction of Al90 compared with Al20. The lower sintering ability of Al200 and Al1000 and the tendency of habit growth are the reasons for the low density of these samples.

Also important is the observation that the density of the samples is not proportional to the particle size. As a rule, the maximal density was obtained when the particle size is about 10 μm . Further growth of the particles size does not lead to an increase in the density.

It could be summarized that $\text{Al}_2(\text{WO}_4)_3$ with initial particle size of 90 nm has the highest compaction level of 80%. The thermal treatment time required for this level of compaction is 10 h at 800°C, 5 h at 900°C and 1 h at 1000°C.

In accordance with the results obtained by sintering $\text{Al}_2(\text{WO}_4)_3$, $\text{Sc}_2(\text{WO}_4)_3$, $\text{In}_2(\text{WO}_4)_3$, $\text{AlSc}(\text{WO}_4)_3$ and $\text{AlIn}(\text{WO}_4)_3$, samples with particle sizes of 20 and 90 nm were investigated. The obtained data qualitatively repeated the previous results. Again, it was observed that:

The density of the samples increases on increasing the sintering time. The required maximum time decreases at higher temperatures.

The average particle size increases on increasing the time and temperature of sintering. The maximum density increases in parallel with the growth in particle size up to 5 - 10 μm . Further increase in the particle size does not result in further compaction of the ceramics.

Highest compaction is achieved when a starting material with particle size of 90 nm is used.

Data for the density, particle size and anisometricity of the tungstates after sintering at 800°C for 1, 5 and 10 h are shown in **Table 1**. The obtained results qualitatively repeat the previous ones, with an exception for $\text{In}_2(\text{WO}_4)_3$. Compared to other tungstates, the particle size of $\text{In}_2(\text{WO}_4)_3$ increases more slowly and it is practically isometric. Probably that is the reason for the achievement of 85% density in cold pressing of 90 nm $\text{In}_2(\text{WO}_4)_3$ after 10 h thermal treatment at 800°C. **Figure 5** presents the particle size and the shape of $\text{Al}_2(\text{WO}_4)_3$, $\text{Sc}_2(\text{WO}_4)_3$ and $\text{In}_2(\text{WO}_4)_3$, treated at the same thermal conditions.

3.2. Hot Pressure Sintering

Starting tungstates of the same chemical compositions and the same average particle size (20, 90 and 200 nm) were subjected to hot pressure sintering. Several combinations of applied temperature and pressure, as well as pressure sintering with stepwise increased temperature and pressure –400°C and 25 MPa for 15 min; 600°C and 50 MPa for 15 min and 800°C and 100 MPa for 15 min were used. Preliminary experiments showed that the duration of pressure sintering can be limited to 1 h. Further

Table 1. Density, average particle size and anisometricity of the tungstates, sintered at 800°C for 1 h, 5 h and 10 h. Me 20 and Me 90 mean $\text{Me}_2(\text{WO}_4)_3$ with initial average particle size 20 and 90 nm respectively. (a) 1 hour treatment; (b) 5 hours treatment; (c) 10 hours treatment.

(a)			
	Relative density [%]	Mean size of the particles [μm]	Anisometricity
Al 20	55.0	0.9	1.0
Al 90	63.2	1.2	1.0
Sc 20	71.0	4.6	1.8
Sc 90	72.3	3.5	1.9
In 20	71.2	0.7	1.0
In 90	72.3	1.7	1.0
AlSc 20			
AlSc 90			
AlIn 20			
AlIn 90			
(b)			
	Relative density [%]	Mean size of the particles [μm]	Anisometricity
Al 20	74.5	1.9	1.8
Al 90	77.7	1.1	1.5
Sc 20	74.5	7.6	3.0
Sc 90	75.8	4.8	3.2
In 20	76.2	2.3	1.0
In 90	75.0	2.0	1.0
AlSc 20	72.1	1.8	1.2
AlSc 90	73.0	5.0	4.0
AlIn 20	71.5	0.7	1.0
AlIn 90	72.3	2.3	1.2
(c)			
	Relative density [%]	Mean size of the particles [μm]	Anisometricity
Al 20	75.3	3.0	2.0
Al 90	81.2	3.8	3.8
Sc 20			
Sc 90	81.0	5.6	2.0
In 20	83.4	3.5	1.0
In 90	85.0	5.2	1.0
AlSc 20	76.8	2.6	1.3
AlSc 90	77.5	6.0	3.0
AlIn 20	76.9	1.1	1.0
AlIn 90	78.1	2.5	1.1

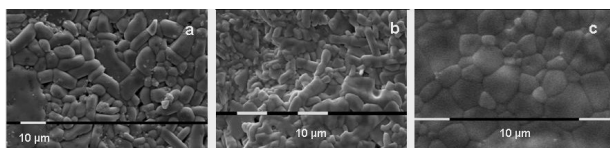


Figure 5. SEM photographs of the surfaces of the $\text{Al}_2(\text{WO}_4)_3$ (a), $\text{Sc}_2(\text{WO}_4)_3$ (b) and $\text{In}_2(\text{WO}_4)_3$ (c) pellets after thermal treatment during 5 h at 800°C .

treatment does not influence the density of the samples. The relative density of the sintered samples of $\text{Al}_2(\text{WO}_4)_3$, $\text{Sc}_2(\text{WO}_4)_3$ and $\text{AlSc}(\text{WO}_4)_3$, depending on the conditions of hot pressure treatment, is shown in **Figure 6**.

It can be seen that hot pressure treatment yields considerably higher density compared with cold pressure treatment. Even after hot pressure sintering at 400°C and pressure 25 MPa, the density reaches almost 90%, while the maximum density achieved in cold pressure treatment and subsequent sintering is about 80%. The density after hot pressure sintering increases with increasing temperature and pressure and reaches 98.6% at 800°C and 100 MPa. It is interesting to note that the stepwise raising of temperature and pressure results in a further increase in the density and the maximum density is 99.6%. The highest density is achieved after treating nanosized powders with an average particle size of 90 nm. The accuracy of the relative density calculation in this case is $\pm 0.02\%$.

The difference between the densities obtained by cold pressing with following sintering and by hot pressure sintering may be explained by the significant increase in the mobility of the grain boundaries in the presence of heat and the limited volume due to the pressure exerted.

SEM photographs throw additional light on the differences in compaction in both compression methods. **Figure 7** presents some typical photographs of the surface of the $\text{Al}_2(\text{WO}_4)_3$ samples after hot pressure sintering under different conditions. Compared with the already shown SEM photographs after cold pressing and subsequent heat treatment, it can be seen that after hot pressure treatment, grains of considerably higher uniformity in size, isometricity and compactness of package are obtained. It is particularly important to note that the $1\ \mu\text{m}$ thick pellets with a density of over 98% are translucent (**Figure 8**). It was found that the transparency is further improved after additional vacuum sintering of the specimens at 1000°C for 2 h. This is probably a result of the additional sealing of the samples, filling of the residual pores and reducing of the phase boundaries.

This result encourages further studies on the optimization of the hot pressure sintering by optimization of the nanoparticles size of the starting powders, the values of temperature and pressure, as well as the sequence of their application, and the conditions for further vacuum sintering.

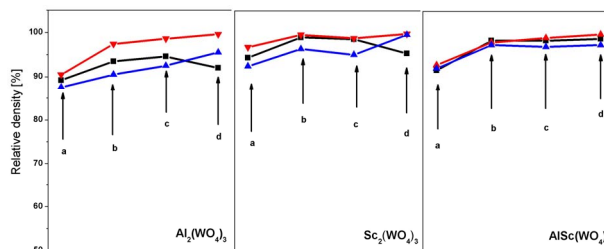


Figure 6. Variation of the relative density of $\text{Al}_2(\text{WO}_4)_3$, $\text{Sc}_2(\text{WO}_4)_3$ and $\text{AlSc}(\text{WO}_4)_3$ pellets depending on the average particle size in the initial pellets (—■— 20 nm, —▼— 90 nm and —▲— 200 nm) after hot pressing under the following conditions: (a) 400°C and 25 MPa, (b) 600°C and 50 MPa, (c) 800°C and 100 MPa after 1 h pressing and (d) stepwise increasing the temperature and pressure: 400°C and 25 MPa for 15 min, 600°C and 50 MPa for 15 min, 800°C and 100 MPa for 30 min.

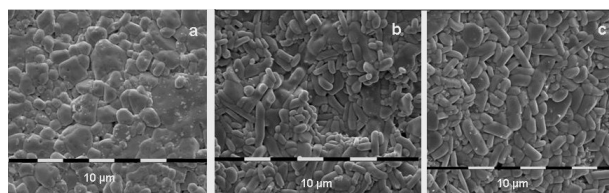


Figure 7. SEM photographs of tungstate ceramics with 90 nm initial average particle size after hot pressing at 600°C and 50 MPa (a); at 800°C and 100 MPa (b) and after stepwise increasing the temperature and pressure: 400°C and 25 MPa for 15 min, 600°C and 50 MPa for 15 min, 800°C and 100 MPa for 30 min (c).



Figure 8. $\text{Al}_2(\text{WO}_4)_3$ ceramics with different levels of transparency obtained after hot pressing.

4. Conclusions

From the results of obtaining $\text{Al}_{2-x}\text{Me}_x(\text{WO}_4)_3$ high density ceramics, where Me = Sc or In, and x varies from 0 to 2, the following conclusions can be drawn:

- Obligatory condition for obtaining high density tungstate ceramics is the availability of initial powders with nanosized particles. These powders have a high level of sinterability which determines a faster grain growth and a high level of compaction.

- The optimal particle size for obtaining high density ceramics is about 90 nm. Grains sized below 90 nm display higher anisometricity; grains sized above this value have low sintering ability. In both cases the preparation of high density ceramics is hampered.

- The densities of 99.8%, obtained by hot pressure sintering, significantly exceed those, obtained by cold pressure sintering.

-High density pellets (98%) have some level of transparency. It could be expected that translucency can be increased by additional optimization of the hot pressure sintering conditions.

REFERENCES

- [1] K. Nassau, H. J. Levinstein and G. M. Loiacono, "A Comprehensive Study of Trivalent Tungstates and Molybdates of the Type $\text{L}_2(\text{MO}_4)_3$," *Journal of Physics and Chemistry of Solids*, Vol. 26, No. 12, 1965, pp. 1805-1816. [http://dx.doi.org/10.1016/0022-3697\(65\)90213-1](http://dx.doi.org/10.1016/0022-3697(65)90213-1)
- [2] N. Imanaka, Y. Kobayashi, S. Tamura and G. Adachi, "Trivalent Al^{3+} Ion Conduction in $\text{Al}_2(\text{WO}_4)_3$ Solids," *Electrochemical and Solid-State Letters*, Vol. 1, No. 6, 1998, pp. 271-273. <http://dx.doi.org/10.1149/1.1390709>
- [3] N. Imanaka, M. Kamikawa, S. Tamura and G. Adachi, "Carbon Dioxide Gas Sensing with the Combination of Trivalent Sc^{3+} Ion Conducting $\text{Sc}_2(\text{WO}_4)_3$ and O^{2-} Ion Conducting Stabilized Zirconia Solid Electrolytes," *Solid State Ionics*, Vol. 133, No. 3-4, 2000, pp. 279-285. [http://dx.doi.org/10.1016/S0167-2738\(00\)00751-7](http://dx.doi.org/10.1016/S0167-2738(00)00751-7)
- [4] G. Adachi, N. Imanaka and S. Tamura, "Rare Earth Ion Conduction in Solids," *Journal of Alloys and Compounds*, Vol. 323-324, No. 12, 2001, pp. 534-539. [http://dx.doi.org/10.1016/S0925-8388\(01\)01138-0](http://dx.doi.org/10.1016/S0925-8388(01)01138-0)
- [5] J. S. O. Evans, T. A. Mary and A. W. Sleight, "Negative Thermal Expansion in a Large Molybdate and Tungstate Family," *Journal of Solid State Chemistry*, Vol. 133, No. 2, 1997, pp. 580-583. <http://dx.doi.org/10.1006/jssc.1997.7605>
- [6] T. A. Mary and A. W. Sleight, "Bulk Thermal Expansion for Tungstates and Molybdates of the Type $\text{A}_2\text{M}_3\text{O}_{12}$," *Journal of Materials Research*, Vol. 14, No. 3, 1999, pp. 912-915. <http://dx.doi.org/10.1557/JMR.1999.0122>
- [7] T. Sugimoto, Y. Aoki, E. Niwa, T. Hashimoto and Y. Morito, "Thermal Expansion and Phase Transition Behavior of $\text{Al}_{2-x}\text{M}_x(\text{WO}_4)_3$ (M = Y, Ga and Sc) Ceramics," *Journal of the Ceramic Society of Japan*, Vol. 115, No. 1339, 2007, pp. 176-181. <http://dx.doi.org/10.2109/jcersj.115.176>
- [8] R. K. Sviridova, V. I. Voronkova and S. S. Kvitka, " Cr^{3+} Doped $\text{Al}_2\text{O}_3 \cdot 3\text{WO}_3$ Crystal Spectra at 290-4.2°K," *Crystrallographia*, Vol. 15, No. 5, 1970, pp. 1077-1078.
- [9] K. Petermann and P. Mitzscherlich, "Spectroscopic and Laser Properties of Cr^{3+} -Doped $\text{Al}_2(\text{WO}_4)_3$ and $\text{Sc}_2(\text{WO}_4)_3$," *IEEE Journal of Quantum Electronics*, Vol. 23, No. 7, 1987, pp. 1122-1126. <http://dx.doi.org/10.1109/JQE.1987.1073477>
- [10] J. Hanuza, M. Maczka, K. Hermanowicz, M. Andruszkiewicz, A. Pietraszko, W. Strek and P. Deren, "The Structure and Spectroscopic Properties of $\text{Al}_{2-x}\text{Cr}_x(\text{WO}_4)_3$ Crystals in Orthorhombic and Monoclinic Phases," *Journal of Solid State Chemistry*, Vol. 105, No. 1, 1993, pp. 49-69. <http://dx.doi.org/10.1006/jssc.1993.1193>
- [11] Y. Kobayashi, N. Imanaka and G. Adachi, "Flux Growth of $\text{Sc}_2(\text{WO}_4)_3$ Single Crystals," *Journal of Crystal Growth*, Vol. 143, No. 3-4, 1994, pp. 362-364. [http://dx.doi.org/10.1016/0022-0248\(94\)90078-7](http://dx.doi.org/10.1016/0022-0248(94)90078-7)
- [12] N. Imanaka, M. Hiraiwa, S. Tamura, G. Adachi, H. Dabkowska and A. Dabkowski, "Single Crystal Growth of Aluminum Tungstate-Scandium Tungstate Solid Solution Samples by the Modified Czochralski Method," *Journal of Crystal Growth*, Vol. 200, No. 1-2, 1999, pp. 169-171. [http://dx.doi.org/10.1016/S0022-0248\(98\)01407-9](http://dx.doi.org/10.1016/S0022-0248(98)01407-9)
- [13] A. Dabkowski, H. A. Dabkowska, J. E. Greedan, G. Adachi, Y. Kobayashi, S. Tamura, M. Hirakawa and N. Imanaka, "Crystal Growth of Aluminum Tungstate $\text{Al}_2(\text{WO}_4)_3$ by the Czochralski Method from Nonstoichiometric Melt," *Journal of Crystal Growth*, Vol. 197, No. 4, 1999, pp. 879-882. [http://dx.doi.org/10.1016/S0022-0248\(98\)00928-2](http://dx.doi.org/10.1016/S0022-0248(98)00928-2)
- [14] N. Imanaka, M. Hiraiwa, G. Adachi, H. Dabkowska and A. Dabkowski, "Thermal Contraction Behavior in $\text{Al}_2(\text{WO}_4)_3$ Single Crystals," *Journal of Crystal Growth*, Vol. 220, No. 1-2, 2000, pp. 176-179. [http://dx.doi.org/10.1016/S0022-0248\(00\)00771-5](http://dx.doi.org/10.1016/S0022-0248(00)00771-5)
- [15] D. Ivanova, V. Nikolov and P. Peshev, "Crystallization Conditions of $\text{Al}_{2-x}\text{Me}_x(\text{WO}_4)_3$, Me = Ga, In, Sc, Yt) Solid Solutions from the Systems $\text{Na}_2\text{O}-\text{Al}_2\text{O}_3-\text{Me}_2\text{O}_3-\text{WO}_3$," *Journal of Crystal Growth*, Vol. 308, No. 1, 2007, pp. 84-88. <http://dx.doi.org/10.1016/j.jcrysgro.2007.08.004>
- [16] D. Ivanova, V. Nikolov and P. Peshev, "Solvents for Growing of $\text{Al}_2(\text{WO}_4)_3$ Single Crystals from High Temperature Solutions," *Journal of Alloys and Compounds*, Vol. 430, No. 1-2, 2007, pp. 356-360. <http://dx.doi.org/10.1016/j.jallcom.2006.05.028>
- [17] D. Ivanova, V. Nikolov and R. Todorov, "Single Crystals Growth and Absorption Spectra of Cr^{3+} Doped $\text{Al}_{2-x}\text{In}_x(\text{WO}_4)_3$ Solid Solutions," *Journal of Crystal Growth*, Vol. 311, No. 13, 2009, pp. 3428-3434. <http://dx.doi.org/10.1016/j.jcrysgro.2009.03.033>
- [18] A. Krell, J. Klimke and T. Hutzler, "Transparent Compact Ceramics: Inherent Physical Issues," *Optical Materials*, Vol. 31, No. 8, 2009, pp. 1144-1150. <http://dx.doi.org/10.1016/j.optmat.2008.12.009>
- [19] S. N. Bagayev, V. V. Osipov, M. G. Ivanov, V. I. Solomonov, V. V. Platonov, A. N. Orlov, A. V. Rasuleva and S. M. Vatnik, "Fabrication and Characteristics of Neodymium-Activated Yttrium Oxide Optical Ceramics," *Optical Materials*, Vol. 31, No. 5, 2009, pp. 740-743. <http://dx.doi.org/10.1016/j.optmat.2008.03.018>
- [20] J. Li, Y. Wu, Y. Pan, W. Liu, L. Huang and J. Guo, "Fabrication, Microstructure and Properties of Highly Transparent Nd:YAG Laser Ceramics," *Optical Materials*, Vol. 31, No. 1, 2008, pp. 6-17. <http://dx.doi.org/10.1016/j.optmat.2007.12.014>
- [21] J. Li, Y. Wu, Y. Pan, H. Kou, Y. Shi and J. Guo, "Densification and Microstructure Evolution of Cr^{4+} , Nd^{3+} :YAG Transparent Ceramics for Self-Q-Switched Laser," *Ceramics International*, Vol. 34, No. 7, 2008, pp. 1675-1679. <http://dx.doi.org/10.1016/j.ceramint.2007.07.019>
- [22] D. Zhou, Y. Shi, P. Yun and J. J. Xie, "Influence of Precipitates on Morphology and Sinterability of Nd^{3+} : Lu_2O_3 Nanopowders by a Wet Chemical Processing," *Journal of Alloys and Compounds*, Vol. 479, No. 1-2, 2009, pp. 870-

874. <http://dx.doi.org/10.1016/j.jallcom.2009.01.080>
- [23] J. Zhang, L. An, M. Liu, S. Shimai and S. Wang, "Sintering of $\text{Yb}^{3+}:\text{Y}_2\text{O}_3$ Transparent Ceramics in Hydrogen Atmosphere," *Journal of the European Ceramic Society*, Vol. 29, No. 2, 2009, pp. 305-309. <http://dx.doi.org/10.1016/j.jeurceramsoc.2008.03.006>
- [24] A. C. Bravo, L. Longuet, D. Autissier, J. F. Baumard, P. Vissie and J. L. Longuet, "Influence of the Powder Preparation on the Sintering of Yb-Doped Sc_2O_3 Transparent Ceramics," *Optical Materials*, Vol. 31, No. 5, 2009, pp. 734-739. <http://dx.doi.org/10.1016/j.optmat.2008.05.004>
- [25] V. Nikolov, I. Koseva, R. Stoyanova and E. Zhecheva, "Conditions for Preparation of Nanosized $\text{Al}_2(\text{WO}_4)_3$," *Journal of Alloys and Compounds*, Vol. 505, No. 2, 2010, pp. 443-449. <http://dx.doi.org/10.1016/j.jallcom.2010.06.100>
- [26] I. Koseva, A. Yordanova, P. Tzvetkov, V. Nikolov and D. Nihtianova, "Nanosized Pure and Cr Doped $\text{Al}_{2-x}\text{In}_x(\text{WO}_4)_3$ Solid Solutions," *Materials Chemistry and Physics*, Vol. 132, No. 2-3, 2012, pp. 808-814. <http://dx.doi.org/10.1016/j.matchemphys.2011.12.016>
- [27] A. Yordanova, I. Koseva, N. Velichkova, D. Kovacheva, D. Rabadjieva and V. Nikolov, "Nanosized Pure and Cr Doped $\text{Al}_{2-x}\text{Sc}_x(\text{WO}_4)_3$ Solid Solutions," *Materials Research Bulletin*, Vol. 47, No. 6, 2012, pp. 1544-1549. <http://dx.doi.org/10.1016/j.materresbull.2012.02.023>